Functional nano-textured titania-coatings with self-cleaning and antireflective properties for photovoltaic surfaces

Maria Grazia Salvaggio [a], Rosalba Passalacqua [a,*], Salvatore Abate [a], Siglinda Perathoner [a], Gabriele Centi [b], Maurizio Lanza [c], Alessandro Stassi [d]

[a] *Dipartimento di Scienze chimiche, biologiche, farmaceutiche ed ambientali, University of Messina and INSTM/CASPE, V.le F. Stagno d'Alcontres 31, 98166 Messina, Italy*

[b] *Dipartimento di Scienze matematiche e informatiche, scienze fisiche e scienze della terra, University of Messina and INSTM/CASPE, V.le F. Stagno d'Alcontres 31, 98166 Messina, Italy*

[c] *Consiglio Nazionale delle Ricerche IPCF, V.le F. Stagno d'Alcontres 37, 98158 Messina, Italy*

[d] *Consiglio Nazionale delle Ricerche ITAE, Via S. Lucia sopra Contesse 5, 98126 Messina, Italy*

Abstract

Photoactive TiO_2-only transparent coatings having self-cleaning and antireflection (AR) properties were prepared by forming first a nanosol through controlled hydrolysis of tetraisopropyl orthotitanate (TIPT), followed by deposition of this nanosol on glass substrates by dip-coating with a final calcination step to form the surface nano-textured thin film. The samples were characterized in terms of nano-structure and -texture by X-ray diffraction, UV–vis spectroscopy, scanning electron microscopy and atomic force microscopy, while AR properties were investigated by transmittance measurements. Self-cleaning properties were analyzed by measuring the changes of water contact angle, and by photocatalytic degradation of a dye. The aim was to analyze how to prepare these materials and the relation of the properties of titania with the surface nano-texture, particularly in relation to obtain the properties required to their use as functional coatings for PV cells. Films with good optical characteristics and high transmittance (<1% loss in transmittance) can be obtained at low speed of dip-coating (6 mm/s) and high nitric acid concentration (0.5 M). Under optimized conditions, calcination at low temperature (400 °C) may already be sufficient to produce coatings with good functional properties, making the procedure compatible with the use of some flexible substrates. A preliminary mechanism of formation of the surface nano-texturing is also proposed.

Keywords: Titanium dioxide; Thin film; Antireflection coatings; Self-cleaning

1. Introduction

The use of photovoltaic (PV) devices to transform directly the solar energy into electrical energy is fast wide spreading to move to a decentralized and more sustainable production of energy. However, this development is posing new problems, because the decentralized use, often on the roof of building in cities, creates the issues of (i) a quick

fouling of the PV devices and (ii) the need to decrease reflective properties to improve light adsorption and especially reduce the visual impact of light reflection.

The top layer of silicon solar cells, the PV cell with wider commercial use, is a cover glass having different functions (Deubener et al., 2009): (i) reduce the high reflection coefficient of silicon to improve cell efficiency, (ii) act as a radiation barrier and optical-coupling element, and (iii) protect against debris and aggressive agents present in air. Surface fouling, particularly in cities and when limited periodic cleaning is possible, still remains an issue and an improvement of antireflection (AR) properties is also generally necessary.

AR properties could be improved by (i) creating appropriate surface profiles (texturing) or (ii) depositing an AR coating, while fouling issues can be minimized by exploiting the photo-catalytic and self-cleaning properties of a cover film (Dobrzański et al., 2012; Goetzberger and Hoffmann, 2005; Dobrzański et al., 2008a,b,c). TiO_2-based thin films are often used as cover layer for PV cells, due to titania properties of (i) high photo-reactivity (Schiavello, 1988; Pelizzetti and Sepone, 1989; Fujishima et al., 1999) and -stability, (ii) super-hydrophilic behavior during irradiation, (iii) good mechanical, chemical and thermal resistance, (iv) low toxicity and cost as well (Gronet and Truman, US Patent 0,017,567 Jan 25, 2007; Gensler et al. US Patent 8,367,579 B2 Feb 5, 2013; Fujishima et al. US Patent 6,387,844 B1 May 14, 2002). The photocatalytic properties of TiO_2 and the hydrophilic effect caused by UV irradiation are well known aspects of the surface chemistry and reactivity of titania (Yates, 2009; Long et al., 2010; Taga, 2009; Zhao et al., 2008; Fujishima and Zhang, 2006). These two aspects are related. Yates (2009) suggested that photoinduced hydrophilicity in titania is due to the photo-oxidation of a non-wetting monolayer of adsorbed hydrocarbon molecules. This monolayer of adsorbed hydrocarbon molecules is initially present over the entire surface, being in equilibrium with the gas phase hydrocarbon. When photooxidation is initiated, the adsorbed hydrocarbon will slowly decrease in the region external to the droplet edge, permitting the water droplet to wet the external surface. The hydrocarbon layer under the droplet is not photooxidized because the water bulk shields this surface from extensive exposure to O_2. Therefore, the contact angle decreases, with a change from hydrophobic-like to hydrophilic-like characteristics of TiO_2 film during UV exposure.

However, much less investigated is how to obtain multifunctional photoactive self-cleaning and AR films, which should combine various additional properties to photoreactivity and photoinduced hydrophilicity: high optical properties of transmittance, AR properties, good mechanical resistance to scratches, and good adherence to glass substrate. In addition, the method of preparation has to be low cost and easily scalable for industrial production.

The specific functional characteristics of TiO_2 are closely related to its crystal structure and morphology, which depend on many factors: manufacturing method, process conditions and final heat treatment. (Centi and Perathoner, 2009a, 2012) However, the relation of these parameters with the nano-texture of the surface is typical not analyzed (Centi and Perathoner, 2009b; Ampelli et al., 2008), although it is known that an efficient self-cleaning requires a specific surface roughness to minimize the contact angle of water drops (lotus effect) and allow the efficient removal of the deposited dust particles during raining. These characteristics should be combined to an efficient photocatalytic activity, related to semiconductor properties of titania, in order to reduce (by photo-oxidation) the accumulation of grease, hydrocarbons and other contaminants on the surface. These contaminants will not only cause a lowering of the transmittance, but also reduce the effectiveness of dust removal, with thus a synergetic effect.

AR properties are depending on the surface nano-texture aspects as well (Passalacqua et al., 2014; Blanco et al., 2015), because light scattering depends on surface roughness (Harada et al., 2013) and nano-texture (Attia et al., 2002). Optical properties of the films, including transparency, are indirectly dependent on the surface roughness. The latter is related to the way the thin film is prepared (nucleation rate, film thickness, etc.) (Harada et al., 2013). These parameters influence also the optical properties of the coating (Blanco et al., 2015). The properties and behavior of titania thin films to be used with optimal performances in photovoltaic glass surfaces may thus depend in a complex way from the preparation, which in turn influences various properties (including surface nano-texture) and related functional properties (self-cleaning and AR behavior, transparency, etc.). However, there are no specific studies concerning the relation of the above properties with the surface nano-texture of titania, particularly in relation to obtaining the multifunctional properties required to their use as functional coatings for PV cells.

Many recent papers have been published on the self-cleaning and/or AR properties of titania-based thin films coatings, for example prepared by thermal evaporation and cathodic arc plasma deposition (Bedikyan et al., 2013), spray pyrolysis deposition of WO_3–TiO_2 nanoparticle (Noh and Myong, 2014), self-assembly of a block-copolymer in combination with silica-based sol–gel chemistry and preformed TiO_2 nanocrystals (Guldin et al., 2013), chemical vapor deposition of SiO_2–TiO_2 thin films (Klobukowski et al., 2013), deposition of a polyimide–titania hybrid film prepared using nano-crystalline titania (Yen et al., 2013), RF magnetron sputtering of titania (Abdullah et al., 2013), anodization of a Ti layer deposited by sputtering technique (Manea et al., 2013), dip-coating in silica-titania colloid solutions (Zhang et al., 2013), layer-by-layer assembly of silica-titania core–shell nanoparticles and silica nanoparticles as building blocks (Li et al., 2013), dip-coating in sol solutions to prepare multilayer SiO_2, TiO_2 and SiO_2–TiO_2 hybrid thin

film (Ye et al., 2013), cluster beam deposition method (Mao et al., 2012) and soft lithography modification of sol–gel glasses (Zhang et al., 2012).

In general, TiO_2 films have been often prepared by physical deposition methods as pulsed laser deposition (Yamamoto et al., 2001), reactive evaporation (Mergel et al., 2000; Zeman and Takabayashi, 2002) and chemical vapor decomposition (Nakamura et al., 2001; Watanabe et al., 2002; Kaliwoh et al., 2002). In these procedures, although applicable on industrial scale, there is a low efficiency of material (Ti-source) utilization, with a consequent impact on costs and sustainability of the preparation process. Solution chemistry methods, such as dip-coating and related techniques (spin-coating, Doctor Blade coating, etc.) have advantages from this perspective (Brinker et al., 1992). As reviewed very recently by Carretero-Genevrier and coworkers (2014), good functional properties (AR, self-cleaning, optical, etc.) in metal oxide thin films, prepared by deposition of sol–gel derived solutions, could be obtained only in hybrid multilayer films. Accordingly, various recent papers on TiO_2-based thin film coatings focused on these aspects, for example the preparation of multilayer films formed by first a mesostructured SiO_2 film followed by a mesoporous TiO_2 film (Yao and He, 2014) or similarly SiO_2–TiO_2 bilayer films (Miao et al., 2013; San Vicente et al., 2012; Chen et al., 2011; Prado et al., 2010), triple layer materials formed by SiO_2, TiO_2 and SiO_2–TiO_2 hybrid thin films (Ye et al., 2013), bilayer films formed by a first Me-functionalized nanoporous SiO_2 film on which a ultrathin crystalline TiO_2 nanoperforated layer is deposited (Faustini et al., 2010; Innocenzi and Malfatti, 2013). These are typically indicated as low-cost methodologies and advantageous over the other type of methodologies cited before. However, in practical applications, e.g. under the presence of cycles of heating/cooling during day and night as well variable degree of humidity, the different expansion characteristics of the layers may induce cracks and film rupture. It is thus preferable to look at the possibility to realize films by sol–gel derived methods composed only of titania. Mu et al. (2012) and Jaguiro et al. (2010) showed that an assembly of TiO_2 nanorods on glass substrate allows obtaining notable AR and self-cleaning properties. However, it is interesting to analyze whether similar properties could be obtained by controlling the preparation parameters in a simple method (easily scale-up) such as the dip-coating procedure with nanosol solutions. Avoiding the need of coating with different materials simplifies the process and reduces the costs, besides to avoid the drawbacks indicated above.

Dip-coating of cover glass with nanosol solutions is one of the preferable methods for creating a thin surface coating by a chemical method. The advantages are the (i) good homogeneity, (ii) easy composition control, (iii) low processing temperature, (iv) large area coating possibility, (v) scalability and low equipment cost. However, the surface nano-texture characteristics of the films prepared by this method have been limitedly investigated, particularly in relation to the preparation of coating films for cover glasses in PV devices (Manea et al., 2013; Chen et al., 2013; Singh et al., 2012; Shimizu et al., 2012; Fleury et al., 2012; Lai et al., 2012; Seo et al., 2010; Kim et al., 2010).

Aim of this work is to investigate the role of the preparation parameters in obtaining, by dip-coating of nanosol solutions, TiO_2-only thin films having the specific surface nano-texture and the other characteristics to make them suitable for their use as transparent functional surface coatings for PV cells. The surface morphology, optical properties and roughness of TiO_2 thin films are analyzed by using different methods: scanning electron microscopy, atomic force microscopy and UV/Vis spectroscopy, as well as measurements of water droplet contact angle and photocatalytic properties. Specific aspects investigated in the preparation are the calcination temperatures, the number of multiple steps during the dip-coating process, the rate of extraction of the glass during the dip-coating process and the nitric acid (used as catalyst) concentration during the preparation of the nanosol. These are the main critical parameters to control from an industrial preparation perspective.

2. Experimental

2.1. Nanosol preparation and thin film deposition

TiO_2 thin films were prepared by the nanosol/dip-coating method. The starting nanosol was prepared through controlled hydrolysis of tetraisopropyl orthotitanate (TIPT, $Ti(C_3H_7O)_4$ 97% from Aldrich) mixed with acetylacetone (AcAc), nitric acid (0.1 or 0.5 M) and absolute ethanol as solvent. The molar ratio of the nanosol composition was: TIPT:AcAc:EtOH:HNO_3 = 1:1:40:1

Nitric acid was used as catalyst, while the water associated to nitric acid solution itself acts as hydrolysis agent for the precursor. Acetylacetone was used as chelating organic ligand. This ligand occupies some of the coordination sites of the alkoxide, thereby lowering the extent and rate of hydrolysis, while at the same time helping in forming a stable nanosol (Dunuwila et al., 1994). The pH value of the nanosol solution is a key factor for controlling the final morphology and thickness of the film (Ghamsari and Bahramian, 2008).

The nanosol is prepared in glove box (under N_2 atmosphere) at r.t. by dropwise addition of absolute ethanol and nitric acid to a solution of TIPT, acetylacetone and ethanol under vigorous stirring. The obtained solution is transparent, yellowish colored and ready for dip-coating procedure in glove box.

Microscope glass slides (75 × 25 × 1 mm) were used for film deposition. Firstly, the glass substrates were carefully ultrasonic cleaned in a mix of acetone/ethanol (1:1) and then in hydrochloric acid 37%. Finally, they were rinsed with distilled water and kept in oven at 110 °C overnight. A home-made dip-coating apparatus was used for the film deposition. The glass substrates were immersed into the

nanosol solution and then withdrawn at different controlled speeds of 6, 10, 24 and 60 mm/s, respectively.

Several films at different acid catalyst concentrations and dip-coating speeds were prepared. Two types of procedures were used: single or multiple (5 times) dip-coatings. In both cases, after each dip-coating procedure, the sample was dried in N_2 atmosphere for 2 h at r.t., kept in a vacuum oven at 200 °C for 1 h and finally calcined at 400, 450 or 500 °C for 1 h. In all cases, transparent TiO_2 thin films were obtained.

The following code will be used to indicate the samples hereinafter: $T_X N_Y C_Z R_K$, where T_X indicates the temperature of calcination (T_{400} indicates a calcination temperature of 400 °C, for example), N_Y the nitric acid concentration ($N_{0.1}$ indicates a 0.1 M HNO_3 concentration used to prepare the nanosol, for example), C_Z the number of times the multiple coating procedure was repeated, as defined before (C_5 indicates that the dip-coating step was repeated 5 times, for example) and R_K indicates the rate used for extracting the sample from the nanosol solution during dip-coating process (R_6 indicates a rate of 6 mm/s, for example).

2.2. Characterization

Glancing incidence X-ray diffraction patterns (G-XRD) of the films were recorded to identify the phase composition and crystallite size. A X-ray diffractometer Philips X-pert 3710 has been used with monochromatic Cu Kα radiation at 40 kV and 30 mA. A 2θ scan rate of 0.02°/s was used. Spectra were collected at 0.5° incident angle. The samples were studied in the range $20° < 2\theta < 80°$. The crystallite size of TiO_2 thin films (Smilgies, 2009) has been estimated from XRD line broadening using the Scherrer equation:

$$L = k * \lambda/\beta * \cos\theta \quad (1)$$

were L is the mean size of the ordered (crystalline) domains of TiO_2 grains present in the thin film, k is a dimensionless shape factor (=0.90), λ is the wavelength of X-ray (Cu Kα = 1.5406 Å), β is the line broadening at half of the maximum intensity after subtracting the instrumental line broadening and θ is the Bragg angle.

Surface morphology and cross-section of the TiO_2 films were examined with Jeol-JSM 5600LV scanning electron microscope (SEM) operating at 20 kV on specimens upon which a thin layer of gold has been previously deposited. For SEM examination of the cross-section, the films deposited on glass were incorporated in a Polifast Phenolic hot mounting resin with carbon filler.

Surface roughness and morphology of the TiO_2 films were evaluated by atomic force microscope (AFM) (Assing Corporation, "Perception" model), operating in contact mode using a pyramidal silicon tip with a nominal radius of 2 nm. The necessary image correction, i.e. tilting in the x- and y-direction, and root mean square roughness (RMS) calculation were carried out using the AFM Gwyddion software. RMS is a function that takes the square of the measures. The RMS roughness of a surface is similar to the roughness average, with the only difference being the mean squared absolute values of surface roughness profile. The roughness average is the arithmetic mean of the absolute values of the height of the surface profile $Z(x)$, with respect to the position (x) of the sample over the evaluation length "L" (De Oliveira et al., 2012):

$$\mathrm{RMS} = \sqrt{\frac{1}{L}\int_0^L |Z^2(x)|dx} \quad (2)$$

Transmittance spectra were recorded in the 200–1500 nm range using a Jasco V-570 UV/VIS/NIR spectrophotometer equipped with an integrating sphere mod. ISN-470 to determine the optical properties ($T\%$), the refractive index (n) and the film thickness (d). The film thickness (d) was estimated from Eq. (3) (Sreemany and Sen, 2004, 2007):

$$d = \frac{1}{n}\left[(2m+1)\frac{\lambda}{4}\right] \quad (3)$$

were m (=0, 1, 2, 3, ...) is the order of $T_{min\ abs}$ and n = the refractive index. The refractive index (n) of the film corresponding to the wavelength (λ) at absolute minimum transmittance ($T_{min\ abs}$) position may be determined by Eq. (4) (Sreemany and Sen, 2004, 2007), while n_0 (1, air) and n_2 (1.515, glass substrate) values are known.

$$n = \sqrt{n_0 n_2}\left(\frac{1+\sqrt{1-T_{min}}}{\sqrt{T_{min}}}\right) \quad (4)$$

The photo-catalytic activity of TiO_2 films were tested under light irradiation simulating the solar spectrum (AM 1.5G, 100 mW/cm^2) on films soiled with methyl orange (MO), a model compound for the contamination by organic pollutants. After depositing (in the dark) a 10^{-5} M aqueous solution of MO on the TiO_2 film surface and air-drying, the film was irradiated with simulated visible light and transmittance spectra, at regulated time intervals, were recorded and compared with data obtained from a bare glass surface contaminated in the same way. The amount of residual MO on the surface of titania film was determined from calibration curves of increase of transmittance (with respect to bare glass) as a function of the amount of MO deposited on it.

The surface wettability was evaluated by measuring the contact angle of water droplets deposited on the film surface under ambient conditions and the acquired data were elaborated with a Matlab software.

3. Results

3.1. Crystalline structure and morphology

The titania coating layer has a smooth, transparent, compact and crack-free appearance, together with a good adherence on the glass substrate. G-XRD characterization

was used to analyze phase composition and crystallite size of the coating titania films. The G-XRD patterns for $T_XN_{0.5}C_5R_6$ films are shown in Fig. 1, where x ranges from 400 to 500 °C. The XRD pattern for the glass substrate is also shown for comparison, evidencing that the very broad background reflection in the 20–40° 2θ range is related to (amorphous) glass substrate itself. Similar XRD patterns were obtained for $T_XN_{0.1}C_5R_6$ samples.

G-XRD results indicate that the TiO_2 thin film calcined at 300 °C is still amorphous (not shown here), while at 400 °C a crystalline phase starts to appear, with a slight intensification and sharpening of reflections increasing the temperature from 400 to 500 °C. Reflections are observed at 2θ values of 25.28°, 37.80°, 48.05°, 53.89° and 55.06° corresponding to the presence of only the anatase phase of TiO_2, (101, 004, 200, 105 and 211 lattice planes, respectively). Similar observations have also been reported in the literatures (Mosaddeq-ur-Rahman et al., 1996; Nishide et al., 2000; Kim et al., 2002).

The results of grain size determination (based on G-XRD data) as a function of preparation parameters are shown in Table 1.

At a fixed calcination temperature, the size of crystallites decreases when the nitric acid concentration for the nano-sol preparation increases, as also found by other authors for different applications (Jin et al., 2010). Instead, a minor effect of the temperature of calcination could be noted, although the effect of calcination temperature is more market in the sample prepared with the higher concentration of nitric acid.

Table 1 reports also the surface roughness (RMS) determined by atomic force microscopy (AFM) measurements in these samples (average values of several scans on 5 × 5 μm area). Although intuitively may be expected that smaller crystallite size leads to lower RMS values, as was observed from other authors although for larger grains (Klobukowski et al., 2013), we observed the opposite effect (Table 1). It may be noted, however, that RMS values are

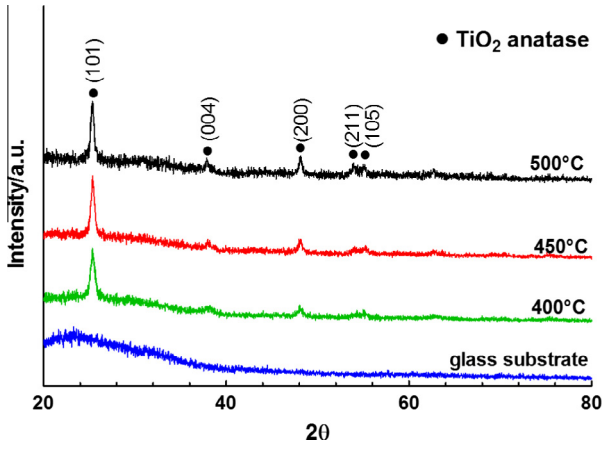

Fig. 1. G-XRD patterns for $T_XN_{0.5}C_5R_6$ films, where X ranges from 400 to 500 °C. The XRD pattern of the glass substrate is also shown for comparison.

Table 1
Influence of preparation parameters on grain size (nm, ±2) and roughness (RMS, nm ±0.1) of the TiO_2 thin film. RMS was the average value of several measurements by AFM on 5 × 5 μm area.

Sample	$T_XN_{0.1}C_5R_6$		$T_XN_{0.5}C_5R_6$	
T_X (°C)	Grain size	RMS	Grain size	RMS
400	28	0.9	14	1.3
450	29	1.3	18	1.8
500	31	1.5	20	1.9

generally low, below 2 nm. Note that RMS is the mean square of surface roughness profile, e.g. the arithmetic mean of the absolute values of the height of the surface profile, with respect to the position of the sample over the evaluation length, as indicated in the experimental part. RMS is thus a statistical value, but being dependent on the area analyzed, it is necessary to average the value of several scans to have reliable data.

The samples show a specific type of surface roughness, an example of which is shown in Fig. 2 reporting the 3D surface profiles of the TiO_2 films obtained by AFM working in contact mode. Fig. 2 shows, on the top, the image (after correction for background) of the nano-roughness in the film, at relatively large area (4 × 4 μm), to analyze the average situation for the sample, while the images below report zooms, at different magnification, to visualize the details of the nano-roughness. It should be commented that the visual appearance of the film by microscopy is of a smooth surface, crack- and porous-free. However, AFM images show the presence of a specific type of surface nano-texture. The largest part is characterized by the presence of smooth nanocones with typical height in the 2–5 nm range and size around 50–100 nm. Few higher nanocones, with height up to 15–20 nm, are also present. The surface well resembles that which is present on lotus leaves and responsible for superhydrophobicity behavior (Latthe et al., 2014).

Other authors (Yu et al., 2002), also studying TiO_2 thin films prepared by dip-coating by AFM, found different results for samples having average RMS values (1.53 nm) close to those in our samples. They observed the presence of mono-dispersed spherical particles of about 70–80 nm in diameter, although suggested to be formed by aggregates of many small TiO_2 crystallites. The result is a granular microstructure and a flat texture, quite different from that observed in our case.

Although there is an influence of the underlying glass substrate characterized by an own roughness (RMS = 1.30 nm), data in Table 1 show that the surface of titania coating film can vary from lower to higher values of glass substrate roughness. This indicates that the specific influence of glass substrate on the surface roughness of titania overlayer can be considered low on the average.

The morphology and thickness of the TiO_2 films were examined by SEM. Fig. 3a shows that an image of the top part of the film, showing that the surface of the film

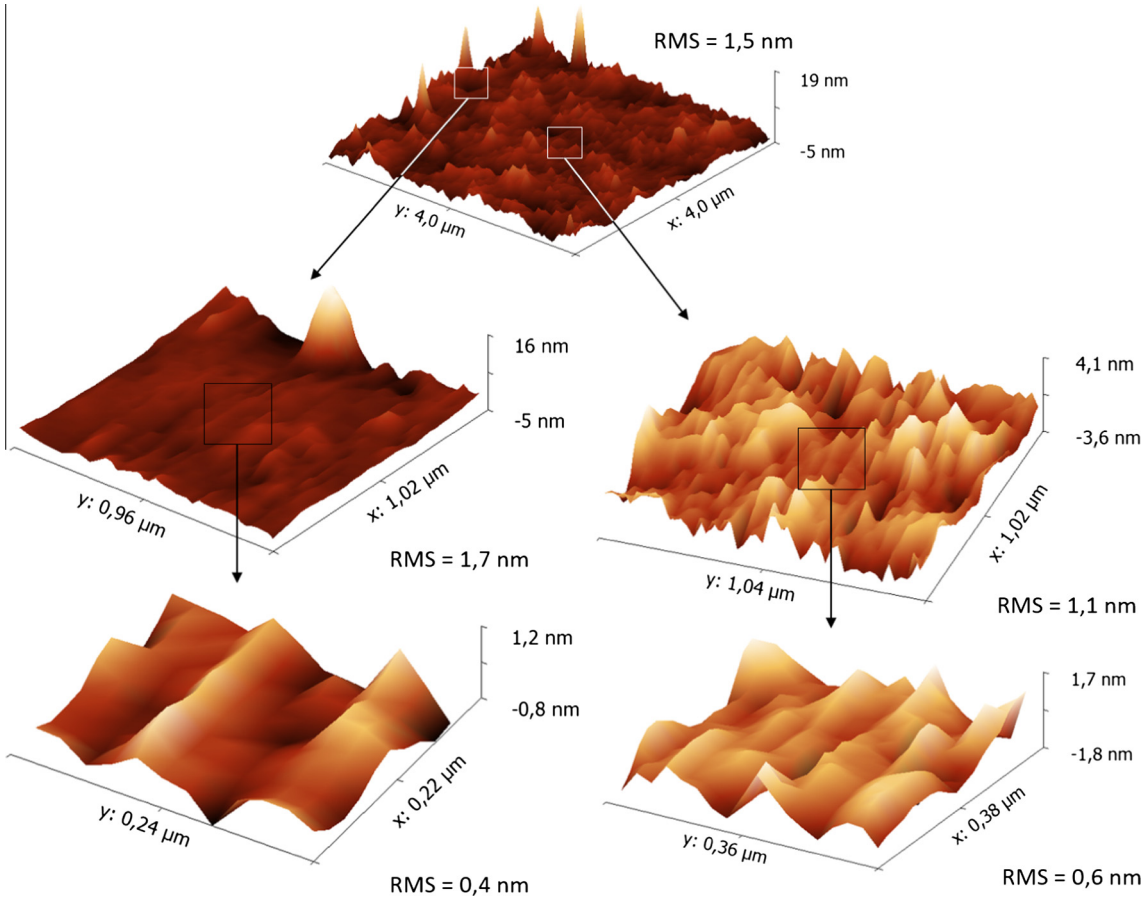

Fig. 2. 3D AFM images of a $T_{500}N_{0.1}C_5R_6$ TiO_2 film, at different zoom magnifications, with the corresponding RMS values.

is smooth, uniform and dense, without the presence of detectable grains or cracks. When the film is mechanically fractured (Fig. 3b), it is possible to evidence the morphology of the underlying film, which has a different structure from the surface, being composed of an agglomerate of particles with average size of 100–150 nm. The thickness of the surface layer is about 10 nm.

The TiO_2 film appears as a dense and compact thin sheet, with thickness of about 400 nm for the C_5 samples. The cross-sectional view (Fig. 3c) shows that the film possesses granular structure. The film thickness was proportional to the number of the dip-coating procedure repetitions ($C_1 \rightarrow C_5$). There is no evidence of separation in layers in this titania film which could mark the steps of the sequential coating procedure. Fig. 3c shows also the good contact with glass substrates, without evidences of delamination of the film. This is confirmed by images (not shown here) at lower magnification. It is possible to observe the absence of voids and cracks in the titania film (confirmed by the analysis of various sections of the film). The presence of surface nano-roughness detected by AFM is confirmed. The good mechanical properties of the film suggested by SEM images (Fig. 3) are confirmed from preliminary scratch tests indicating their mechanical stability and durability. Nanoscratch tests combined with the observation by microscope of the scratch tracks confirm the good adhesion of the titania film, particularly in the samples calcined above 400 °C. The preliminary results are well comparable with those determined for titania thin films prepared by radio frequency magnetron sputtering on glass substrates (Hasan et al., 2010). The critical loads of TiO_2 films is above about 5 N (Newton), with an increase passing from the as deposited to the calcined samples, indicating an improved adhesion of TiO_2 films on glass substrates. Chung et al. (2009) suggested that the enhanced film adhesion by calcination derives from interdiffusion of atoms in the film/substrate interface and densification of the films.

The film thickness determined by SEM measurements (Fig. 3c) is in good agreement with the film thickness determined by the Swanepoel method using the transmittance data (see later).

3.2. Optical properties

Optical transmittance spectra have been recorded in the wavelength range 200–1500 nm. Due to the characteristics of the dip-coating procedure, the titania film is present on both sides of the glass substrate. Thus, the effective transmittance and transparency of the single film will be better. In practical applications, a single surface will be coated.

The optical spectra (Fig. 4) are characterized from a region of high absorbance (minimal transmittance) below

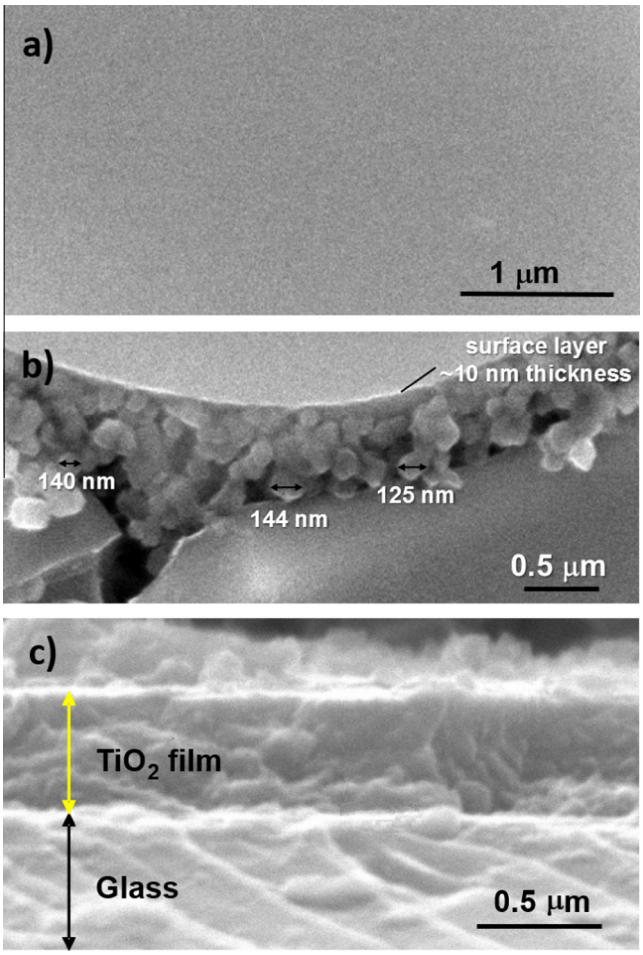

Fig. 3. (a) SEM image of the top view of a $T_{500}N_{0.1}C_5R_6$ titania film, showing the presence of a smooth, compact and crack-free surface. (b) Details of the nano-grains with average size of 100–150 nm present below the smooth surface and which may be evidenced by mechanically fracturing the film. (c) Cross-section of $T_{500}N_{0.5}C_5R_{24}$ titania film.

about 350 nm, where light transmission is cut from the strong absorption of the glass substrate itself (below 350 nm the band gap for titania is also present) and a region above about 600 nm, where *d–d* transitions of titanium ion are present[1].

Some weak interference fringes, in the wavelength range 350–1500 nm, deriving from the interference between the air/thin film and thin film/substrate interfaces, are also present. They depend on the film thickness and characteristics. Fig. 4b shows the region between 400 and 1200 nm amplified to better highlight these interference fringes, which are responsible in some cases of a slight color of the film, ranging from light violet to green or yellow (see web version of Fig. 5).

Fig. 4c reports the spectra in the 300–400 nm region of the samples increasing from one to five times the dip-coating procedure ($C_1 \rightarrow C_5$). The sample with one coating produces a spectrum quite close to that of glass substrate, except for the presence of some interference fringes indicating the presence of a very thin titania film. This is due to the very low amount of titania in this sample, deriving from the weak retention of the titania nanosol the first time the dip-coating process is made. This initial layer, however, acts as "seeding" element for the second dip-coating treatment, where larger amount of titania remains anchored to the surface, as indicated from the drastic increase in the absorption between about 320 and 380 nm. The addition of further layers increases further the absorption in this region, due to the increase of film thickness. However, the increase in absorption from 2nd to 3rd layer and further layers is smaller with respect to that observed between the first and second coating.

It may be also noted that up to three dip-coating procedures, the maximum in this region is observed at about 330 nm, while shifts to about 340 nm for 5 dip-coating procedure. King et al. (2008), studying TiO_2 films prepared by atomic layer deposition, showed the presence of size-dependent quantum confinement in titania films with characteristics comparable to those of our films, although different preparation. Poulopoulos et al. (2011) showed that in copper oxide layer of about 230 μm, a decrease of the thickness leads to a blue shift of the band-gap energy due to quantum confinement effect, confirmed by theoretical calculations. Uchida et al. (2010) showed the presence of weak quantum confinement effects in ordered mesoporous TiO_2 thin films supported on conductive glass. We earlier discussed in detail the presence of modification of the band gap in the 3.0–3.4 eV region in nanostructured thin titania films due to 2D quantum confinement effect (Perathoner et al., 2007). Chiodo et al. (2010) analyzed in detail by full ab initio treatment the electronic and optical properties of TiO_2 demonstrating how a 2D (film) and 1D (nanotube) nanostructure leads to a slight increase in the band gap with respect to bulk TiO_2 anatase. The nanostructure influence on the band gap is related to quantum confinement effect.

Therefore, there are various evidences in literature showing that the band gap of TiO_2 anatase may changes in the 3.0–3.5 eV region, depending on 2D quantum effect and nanostructure. G-XRD data (Fig. 1) showed the presence of only the anatase phase of TiO_2 in these samples, but SEM data show the presence of a very dense and compact thin film on the surface (thickness of about 10 nm) with an underlying structure formed by nanograins. Increasing the number of coatings, the underlying structure becomes dominant with respect to the first one. It is reasonable that the observed slight band-gap shift (Fig. 4c) by increasing the number of coatings may be thus attributed to 2D quantum confinement related to the change in the specific nanostructure of titania layer, although further studies are necessary to further clarify this aspect.

With respect to the cleaned glass substrate (transmittance at 550 nm of 97.3%), $T_{500}N_{0.5}C_ZR_6$ samples (C_1 and C_5) show transmittance of 96.6% and 96.4%, respectively.

[1] For interpretation of color in Fig. 4, the reader is referred to the web version of this article.

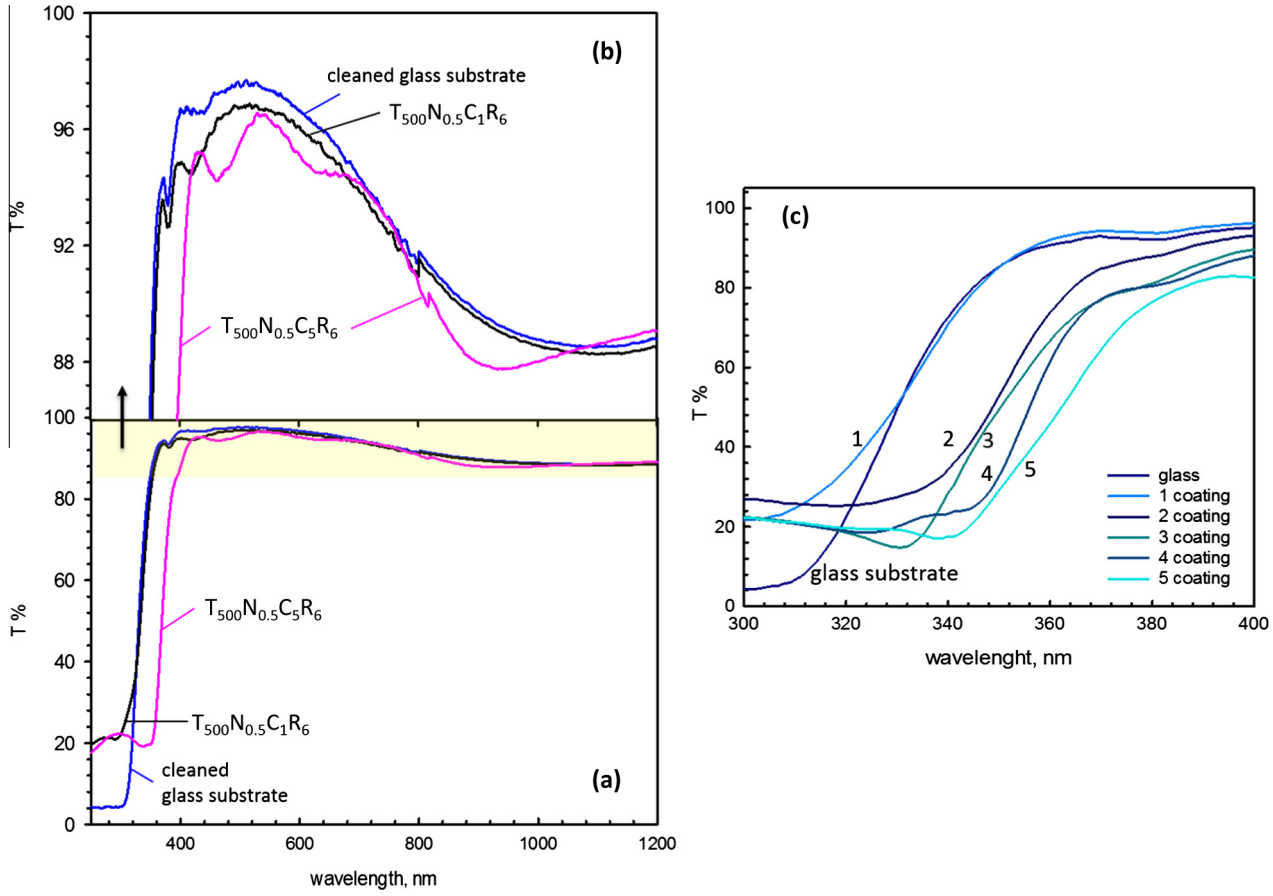

Fig. 4. (a) Transmittance spectra of cleaned glass substrate and $T_{500}N_{0.5}C_ZR_6$ samples, where $Z = 1$ or 5. (b) Amplified region with the higher transmittance. (c) Transmittance spectra in the 300–400 nm region of cleaned glass substrate and $T_{500}N_{0.5}C_ZR_6$ samples, where Z increases from 1 to 5.

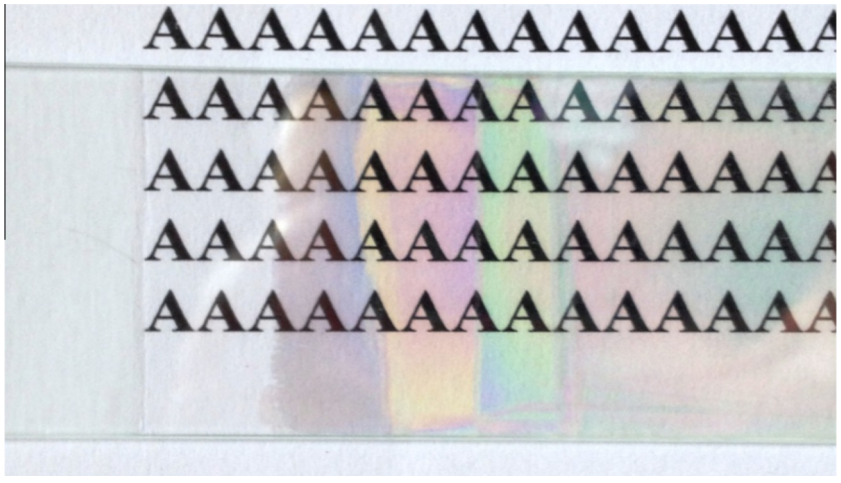

Fig. 5. Photo of $T_{500}N_{0.5}C_5R_6$ sample, showing on the background alphabetic letters to evidence the transparency of the film.

This small decrease of transmittance can be further improved using higher concentrations of nitric acid during nanosol preparation, as discussed later. The increase of the coating layers ($C_1 \rightarrow C_5$) increases the number of fringes, consistently to the increase of film thickness. By taking into consideration the absorbance of the glass substrate itself and that the titania film is present on both sides of the glass substrate, the transparency of these TiO_2 films is excellent, with less than about 1% loss of transmittance even in the five times coated samples. This is related to the characteristics of the films and the presence of small grains. The transparency of the TiO_2 films is shown also in Fig. 5 reporting the photo of $T_{500}N_{0.5}C_5R_6$ sample overlapped to a background of alphabetic letters.

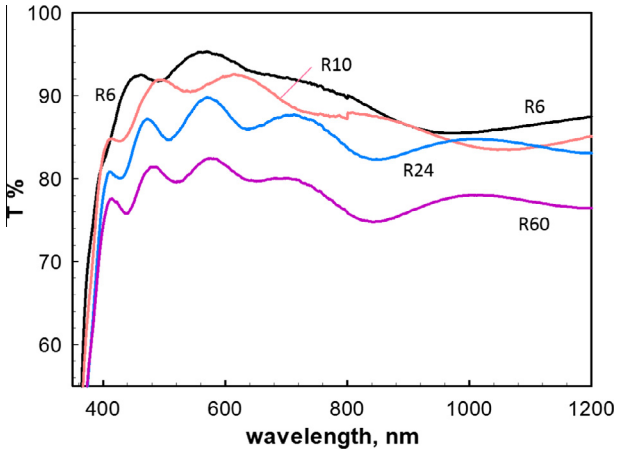

Fig. 6. Influence of dip-coating speed on optical spectra for $T_{500}N_{0.1}C_5R_K$ samples (K varies from 6 to 60 mm/s).

Table 2
Titania film thickness (d, nm ±5), refractive index (n) of the film corresponding to the wavelength (λ, nm ±1) at absolute minimum transmittance ($T_{\min\ abs}$) for $T_{500}N_{0.1}C_5R_K$ samples (K varies from 6 to 24 mm/s).

Speed (mm/s)	λ	$T_{\min\ abs}$	n	d
6	969	0.8685	1.802	403
10	1102	0.8443	1.868	442
24	1284	0.8087	1.967	490

3.3. Influence of dip-coating speed

Fig. 6 reports the optical spectra of $T_{500}N_{0.1}C_5R_K$ samples, where the rate used for extracting the sample from the nanosol solution during dip-coating process (R_K) varies from 6 to 60 mm/s. There is a decrease of transmittance (increase of absorbance) as the speed of extraction increases during the dip-coating procedure. The same behavior is observed for both 1-coated and 5-coated films ($C_1 \rightarrow C_5$). Calculation of film thickness using transmittance spectra (Table 2) evidences the increase of film thickness (d) when dip-coating speed increases. The interference fringes become also more intense and vary in frequency, consistently with the change of film characteristics.

Table 2 also shows that the antireflection behavior (AR), related to the refractive index n, is favored in case of thinner films. The best optical properties and AR behavior are obtained at the lowest dip-coating speed, e.g. for thinner films in 5-coating samples (C_5). A minimum thickness, above about 200 nm, is necessary to obtain good mechanical adherence of the titania coating on the glass substrate. For this reason, multiple coating was typically used here with respect to single coating. It may be also observed that AR properties of these films are well comparable with those of more complex hybrid multilayer coatings (Ye et al., 2013; Faustini et al., 2010; Innocenzi and Malfatti, 2013).

Table 3
Titania film thickness (d nm ±5), refractive index (n) of the film corresponding to the wavelength (λ nm ±1) at absolute minimum transmittance ($T_{\min\ abs}$) for $T_XN_{0.5}C_5R_{10}$ samples (X varies from 400 to 500 °C).

T (°C)	λ	$T_{min\ abs}$	n	d
500	1060	0.8630	1.815	438
450	1077	0.8621	1.817	444
400	1145	0.8461	1.863	461

Moreover, Table 2 evidences that the refractive index n increases with the dip-coating speed, as also observed by other authors (Attia et al., 2002; Blanco et al., 2015). This is caused by a decrease in film porosity (more dense nanoparticles packing), and by a corresponding increase in film thickness with dip-coating speed.

3.4. Influence of calcination temperature

There are no significant differences in the transmittance spectra of TiO_2 films, deposited at low dip-coating speed and calcined at different temperatures in the 400–500 °C range. As reported in Table 3, the transmittance increases slightly with calcination temperature and reach a maximum at 500 °C. The same findings have been observed for films deposited from the nanosol prepared with 0.1 M concentration of nitric acid. Therefore, a calcination temperature of 400 °C may be sufficient to obtain high optical properties in the TiO_2 thin films. This is important because 400 °C is the temperature limit for some flexible polymer-based substrates, while lower calcination temperatures do not allow obtaining a good crystallinity in the titania (lowering photocatalytic properties).

3.5. Influence of HNO_3 concentration during nanosol preparation

The influence of HNO_3 concentration during nanosol preparation on the optical properties of $T_{500}N_YC_5R_{24}$ samples is reported in Fig. 7.

The transmittance of the samples increases when HNO_3 concentration during nanosol preparation increases. The interference fringes slightly change frequency and intensity varying nitric acid concentration. The overlap of one of these interferences fringes on the band gap causes the apparent slight change of the latter. The interference fringes are more intense for higher film thicknesses (elevated speed of extraction during dip-coating procedure).

As shown in Table 1, the particle size of TiO_2 crystallites becomes smaller on increasing nitric acid concentration during nanosol preparation. It is possible to have a better densification during calcination leading to a thinner film, with a consequent higher transmittance. However, at lower calcination temperatures (450 °C and 400 °C), the influence of nitric acid concentration on transmittance is minor,

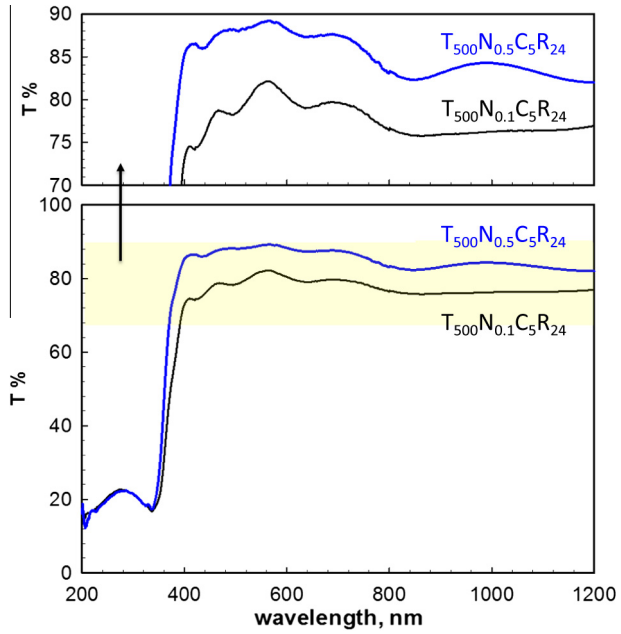

Fig. 7. Influence of acid catalyst concentration on optical spectra of $T_{500}N_YC_5R_{24}$ samples. (b) Amplified region with the higher transmittance.

reasonably due to the not well-organized crystalline structure.

3.6. Photocatalytic activity

Self-cleaning properties of titania coatings also depend on their ability to photocatalytically oxidize the organic substances adsorbed on them, thus preventing the surface fouling by organic species. It is known that titania is photoactive in the oxidation of organic substances in water, when the crystalline anatase phase is present (although small amounts of a second phase such as rutile promotes the activity) (Centi and Perathoner, 2009a, 2012; Schneider et al., 2014; Wang et al., 2014). However, it is necessary to verify whether the titania coating possesses photocatalytic activity, in particular for samples calcined at the lower temperature (400 °C). The rate of photoconversion, differently from depollution procedures, is not a specific issue for the application discussed in this work, because under practical uses, the samples remain exposed to sunlight for long time and the deposition of organic pollutants from atmosphere is a relatively slow process. For this reason, a simple model reaction (photocatalytic degradation of an organic azo-dye, methyl orange – MO) was investigated using simulated solar light (AM 1.5G, 100 mW/cm^2), in order to have also a comparison with literature data on similar materials (boron-doped TiO_2) (Zhang et al., 2012).

The adsorbed MO gives rise to a peak with a maximum centred at 468 nm, which gradually decreased during irradiation process. The amount of residual MO on the surface was determined from the decrease of the intensity of this peak as a function of time, during exposure of the glass substrate coated with the titania film to simulated solar light in air. For reference, the bare glass substrate on which MO was deposited was used to analyze stability of MO in the absence of the titania film. The samples were dried in dark after depositing of the aqueous solution of MO and thus the experiment may give indication on the photocatalytic activity of the titania film under practical conditions. For this reason, water was not used to clean up after or during the exposure to sun light.

The results are reported in Fig. 8 which compares the performances of $T_{400}N_{0.5}C_5R_{24}$ (calcined at 400 °C) with those of $T_{500}N_{0.5}C_5R_{24}$ (calcined at 500 °C) and of the bare glass substrate. The latter shows a negligible activity, indicating that MO does not degrade under the chosen experimental conditions. The symbols in Fig. 8 are the experimental ones, while the lines are calculated from regression analysis using a first order kinetic of degradation, which correctly fit the data in the experimental range investigated.

The rate constants determined from the fitting are reported in Table 4. The results show that the presence of titania coating increases of about two order of magnitude the rate of photocatalytic conversion of adsorbed organic molecules with respect to the bare glass substrate. The calcination at higher temperature leads to better activity, but already at a low calcination temperature (400 °C) a reasonable good activity (about 65% of that of the sample calcined at 500 °C) is present. This is important, because in some applications using flexible covering glasses, a temperature of about 400 °C is the limit for the calcination treatment.

3.7. Contact angle

Contact angle of water drops on titania layers is an important characteristic, because a higher contact angle

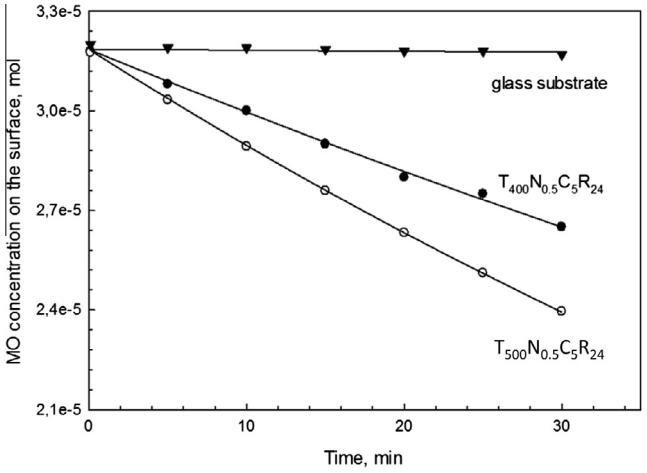

Fig. 8. Photocatalytic conversion of adsorbed methyl orange (MO) in $T_{400}N_{0.5}C_5R_{24}$ and $T_{500}N_{0.5}C_5R_{24}$ samples with respect to bare glass substrate. Symbols are the experimental values and lines calculated from regression using a first order rate of conversion. Irradiation with simulated solar light (AM 1.5G), conversion of MO monitored by measuring the decreasing of the maximum of MO absorption peak, at 468 nm, during irradiation time.

Table 4
First order rate constants of MO conversion determined in experiments reported in Fig. 8. The rates constants were determined from global fitting of the data, considering the initial concentration of MO constant in all the samples and equal to $3.185 \cdot 10^{-5}$ mol. The Rsqr of the fitting was 0.999 and standard error of estimate 1.555E−005.

Sample	1st order rate constant
$T_{400}N_YC_5R_6$	6,13e−3
$T_{500}N_YC_5R_6$	9,53e−3
Bare glass substrate	8,79e−5

(e.g. more spherical drops, better rolling properties) favors the cleaning of the PV during raining from dust particles and other deposits. It this know, as discussed in the introduction, that the irradiation of titania with UV light induces super-hydrophilicity in titania due to the removal by photo-oxidation of adsorbed (non-wetting) hydrocarbons (Yates, 2009). However, a nano-textured surface may reduce the relevance of this photoinduced hydrophilicity still allowing a relatively high contact angle (which favor rolling properties and self-cleaning) with respect to an ideal flat titania surface, for which a complete wetting is present leading to negligible rolling properties. On the other hand, some hydrophilic character of the surface layer may be desirable for a better interaction with the glass substrate and reduce the formation of streaks. A good compromise is for contact angles in the 60–90° region (Yao and He, 2014; Yates, 2009). As an indication, the contact angles of water droplets on vertically-aligned TiO_2 nanotube textured surfaces lie between 84° and 86° (Boinovich et al., 2008).

The contact angle of TiO_2 films obtained from nanosols prepared using different acid concentrations is reported in Table 5 together with the results of root mean square roughness (RMS) determined by AFM measurements and grain size average dimensions, obtained by G-XRD analysis.

Increasing nitric acid concentration during nanosol preparation leads to a decrease of grain size and an increase in surface roughness, as commented before. This effect leads to an increase of the contact angle of water droplets on titania coating layer (eg. an increase of rolling properties), which is positive for self-cleaning characteristics.

In order to better understand this behavior, Fig. 9 reports the 2D profile of surface roughness for the two samples reported in Table 5. The sample prepared from the nanosol with the higher concentration of nitric acid (Fig. 9b) shows a different roughness profile with respect to the other sample. There is in $N_{0.5}$ sample a more regular micro-structure with respect to $N_{0.1}$. This micro-texture favors the air trapping below the liquid and thus changes an hydrophilic surface (like titania) into an hydrophobic one (Li et al., 2007).

Table 5
$T_{500}N_YC_5R_6$ samples, where $Y = 0.1$ or 0.5 M: contact angle (°, ±3), root mean square roughness (RMS nm ± 0.1) and grain size (nm, ±2) average dimensions.

T_{500}–N_Y–C_5–R_6	$N_{0.1}$	$N_{0.5}$
RMS	1.53	1.94
Contact angle	44	60
Grain size	31	20

4. Discussion

Various factors in the preparation by a nanosol/dip-coating procedure (dip-coating speed, acid concentration during nanosol preparation, calcination temperature, multistep dip-coating) affect the functional behavior of titania thin films. Films with good optical characteristics and high transmittance can be obtained at low speed of dip-coating (6 mm/s) and high nitric acid concentration (0.5 M). A calcination temperature of even 400 °C, thus compatible with some flexible substrates, allows having good crystallinity and photocatalytic activity, together with good surface nano-texture for self-cleaning properties. For higher dip-coating speeds (>10 mm/s) it is necessary to make a calcination at 500 °C to obtain high transmittance values.

The increase of nitric acid concentration enhances the nucleation rate and thus smaller size crystalline grains are present in the final film. The smaller crystallite size leads to an increase in RMS (Table 1). The AFM surface plot reveals that the film is rough at the nanoscale level. Fig. 9 further confirms the presence of this nanoscale

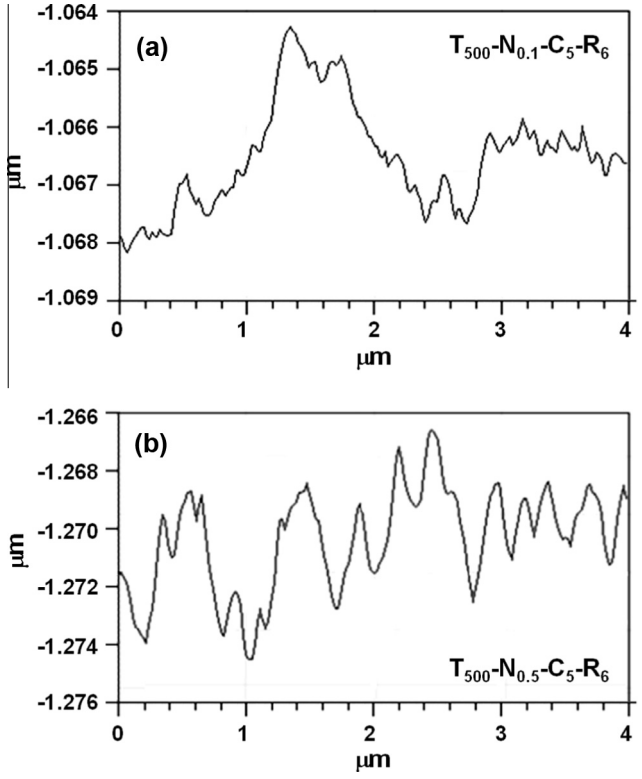

Fig. 9. 2D profile of surface roughness for $T_{500}N_YC_5R_6$ samples, where $Y = 0.1$ (a) or 0.5 (b) M.

roughness, evidencing how the increase in the nitric acid concentration during nanosol preparation leads to smaller grain size, higher RMS and higher contact angle of water drops (Table 5), leading to better self-cleaning properties.

On increasing the nitric acid concentration, smaller average grains are formed, but with a more irregular shape, determining the higher surface nano-roughness. However, as commented before regarding the paper by Yu et al. (2002), different surface nano-morphologies could be obtained by similar analogous dip-coating procedures.

In dip-coating, the substrate is withdrawn vertically from the liquid at a defined speed (u_o) and under a controlled atmosphere (N_2 atmosphere in our case). Fig. 10 shows schematically the process of dip-coating. The liquid film, remaining adherent to the moving substrate due to surface tension, evaporates at a not-constant speed along the axial direction of the substrate (orthogonal with respect to the liquid bath), because the evaporation rate near the drying line results in a parabolic thickness profile. Many factors determine the thickness of the deposited film such as film thickness and position of the stream line dividing the upward and downward fluid moving layers, liquid viscosity, substrate speed, etc. as well as the sol characteristics (Brinker et al., 1991). Therefore, many factors may influence the characteristics of the films obtained by dip-coating. However, an important factor determining the functional properties of the coating film is the surface nano-roughness, as shown in this work. The fundamental studies on the mechanism of thin film formation by dip coating procedure, and in general on the mechanism of film formation in sol–gel based procedures, (Li et al., 2007; Brinker et al., 1991; Brinker and Hurd, 1995; Hurd, 2006; Livage, 2004) do not explain how this surface roughness is created in dip-coating (or related) methodologies and how to control the surface nano-texturing properties. For this reason, as commented in the introduction, the nano-texturing of titania coating is usually made either by introducing hybrid multilayer coatings (with silica or polymers (Innocenzi and Malfatti, 2013; Soler-Illia et al., 2011) or by physical texturing the surface (for example, by rolling mask (Seitz et al., 2014) or nanoimprint (Lee et al., 2013) litography). The results reported here show that it is possible to nano-texturing the surface of a titania-only thin film by controlling the dip-coating procedure. Consequently, it is possible to control the functional properties (AR and self-cleaning behavior) of the surface and optimize the behavior as coating for PV cells.

The film during the dip-coating procedure is formed when the entrained inorganic precursors (sol particles) are concentrated on the surface of the glass substrate by gravitational draining and evaporation, often accompanied by condensation reactions involving hydroxyl ligands to produce M–O–M or M–OH–M bonds between the sol particles (Brinker et al., 1991; Brinker and Hurd, 1995). The increasing concentration forces the precursors into close proximity causing aggregation and gelation, while repulsive particles

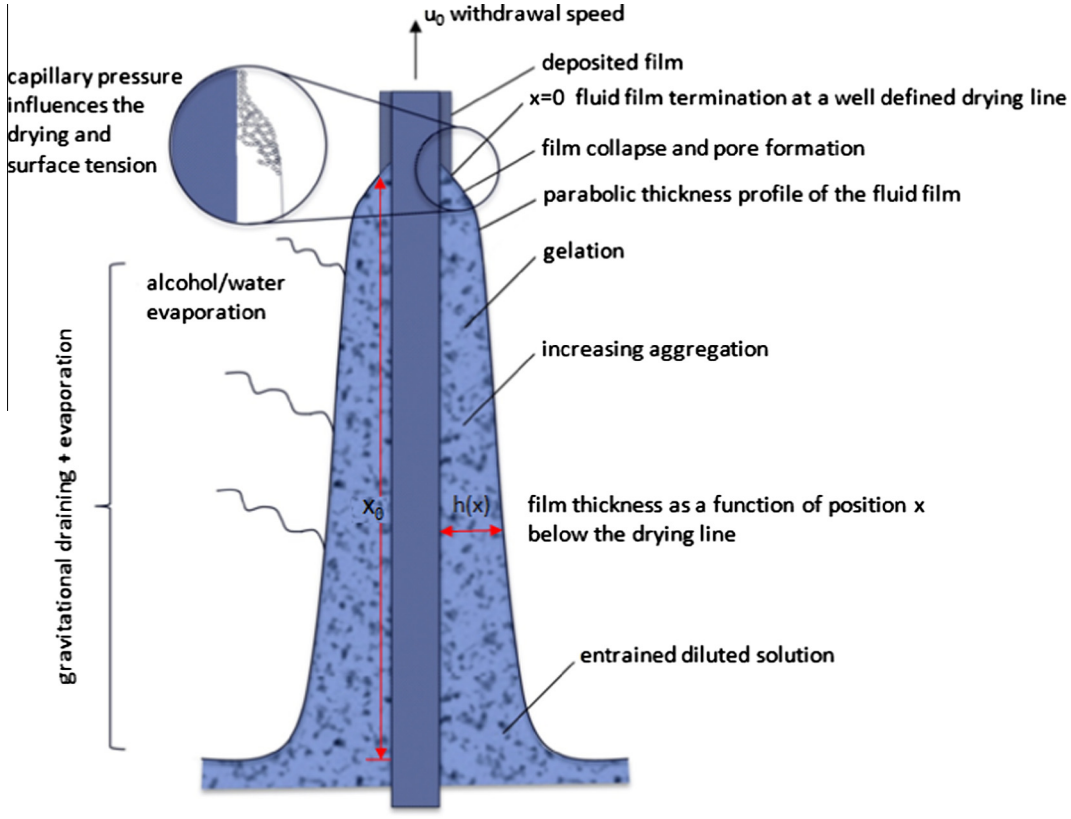

Fig. 10. Schematic cartoon of the dip-coating process.

appear to assemble into liquid- and crystal-like structures depending on withdrawal rate. Competition occurs between solvent evaporation compacting the structure to form nano-aggregates and condensation reactions, which stiffen the structure, increasing its resistance to compaction (Brinker et al., 1991; Brinker and Hurd, 1995; Hurd, 2006). Unlike bulk gel formation, the drying stage overlaps the aggregation-gelation stages, thus allowing only short time (seconds) for condensation reactions to occur. Therefore, capillary forces (due to the pressure created by the liquid–vapor menisci as the nano-aggregate collapse into a film) determine the final stage of thin film formation.

In these conditions, possibly induced also by the presence of nano-roughness on the substrate acting as seeding element, it is reasonable to expect the formation of nano-cones determined from this mechanism, when the result of these forces is vertical with respect to the substrate plane. For this reason, the nano-texturing of the surface of titania film produced by dip-coating depends on the parameters such as dip-coating speed rather than on grain size, as experimentally observed in this work. It is necessary, however, to use nanosols formed by rather small precursor particles to make effective this process, explaining why using larger sol particles this effect was not observed (Yu et al., 2002). For this reason, an important effect is also related to the concentration of catalyst (nitric acid) used in the preparation of the sol, because leads to smaller sol particles favouring above mechanism, and especially the formation of a more regular surface nano-texturing (Fig. 9) which enhances AR and self-cleaning properties, together with high transparency of the film (Fig. 5).

Although this mechanism of surface nano-texturing in titania thin films produced by dip-coating is preliminary (it is out of the scope of this work the analysis of the mechanism), it may serve as initial working hypothesis to understand this process and further optimize it. This work is limited to the demonstration that it is possible to produce useful AR and self-cleaning titania-only films for PV cells using a controlled dip-coating procedure and suitable nanosol characteristics. This technology is relevant to produce low-cost an easy-scalable commercial coatings for PV cells having good AR, self-cleaning and optical properties. As indicated in the introduction, chemical methods have a better efficiency in material utilization with respect to physical methods such as those discussed in the introduction. Between the chemical methods, attention has been largely focused on hybrid surface coatings, but the use of TiO_2-only films has the advantage of a simpler method, that is easy to scale-up and of potentially lower cost.

It may be finally remarked that for optimized conditions of preparation, calcination at low temperature (400 °C) compatible with some flexible polymeric substrates may be sufficient to have good functional properties, opening thus the possibility to use this method in the preparation of AR and self-cleaning coatings for flexible PV cells. Due to the architectural integration of these cells into buildings, AR and self-cleaning properties of cells is an even more important target, but several of the current methods utilized in literature are not suited for this objective.

5. Conclusions

The preparation method described in this work allows obtaining thin, surface nano-textured TiO_2 films with high optical properties of transmittance. The use of these films as functional coatings (having self-cleaning and AR properties) for glasses used in PV cells requires also controlling the surface nano-texture, in addition to optical properties. Aim of this work was to show how various factors in the preparation by a nanosol/dip-coating procedure (dip-coating speed, acid concentration during nanosol preparation, calcination temperature, multistep dip-coating) affect both optical and surface nano-texture properties.

Films with good optical characteristics and high transmittance (<1% loss in transmittance) can be obtained at low speed of dip-coating (6 mm/s) and high nitric acid concentration (0.5 M). Under optimized conditions, calcination at low temperature (400 °C) may be even sufficient to produce coatings with good functional properties, making the procedure compatible with some flexible substrates. For high dip-coating speeds, on the contrary, calcination at higher temperature (500 °C) is instead necessary to obtain good transmittance values of the film.

In conclusion, the control of the preparation parameters in the nanosol/dip-coating method allows preparing titania coatings for the cover glass in PV cells having high transparency and good AR properties, together with suitable surface nano-texture and photocatalytic properties for their use as self-cleaning materials. Preliminary tests also indicate good adherence, stability and mechanical resistance. The preparation procedure allows an efficient utilization of raw materials and can be considered a suitable method for industrial preparation of coating films for PV cells, although further studies may be necessary. The properties depend on the preparation of a specific nano-texturing of the surface of titania-only thin film by controlling the various parameters during the dip-coating procedure, as well as in the preparation of the nanosol. A preliminary mechanism of formation of the surface nano-texturing is also proposed.

Acknowledgments

This work has been realized under the national Program PON R&C 2007-2013, project "FOTOVOLTAICO" (PON01_01725) and the authors gratefully thank the financial support by MIUR.

References

Abdullah, M.H., Mamat, M.H., Zahidi, M.M., Mahmood, M.R., 2013. Transmittance enhanced properties of novel encapsulated ITO/arc-TiO_2 antireflective TCO substrate prepared by RF magnetron sputtering. Adv. Mater. Res. 667, 573–582.

Ampelli, C., Passalacqua, R., Perathoner, S., Centi, G., Su, D.S., Weinberg, G., 2008. Synthesis of TiO_2 thin films: relationship between preparation conditions and nanostructure. Topics Catal. 50, 133–144.

Attia, S.M., Wang, J., Wu, G., Shen, J., Ma, J., 2002. J. Mater. Sci. Technol. 18, 31–33.

Bedikyan, L., Zakhariev, S., Zakharieva, M., 2013. Titanium dioxide thin films: preparation and optical properties. J. Chem. Techn. Metall. 48, 555–558.

Blanco, E., González-Leal, J.M., Ramírez-del Solar, M., 2015. Photocatalytic TiO_2 sol–gel thin films: optical and morphological characterization. Sol. Energy 122, 11–23.

Boinovich, L.B., Emelyanenko, A.M., 2008. Hydrophobic materials and coatings: principles of design, properties and applications. Russian Chem. Rev. 77, 583–600.

Brinker, C.J., Frye, G.C., Hurd, A.J., Ashley, C.S., 1991. Fundamentals of sol–gel dip coating. Thin Solid Films 201, 97–108.

Brinker, C.J., Hurd, A.J., 1995. Fundamentals of sol–gel dip-coating. Ceram. Trans. 55, 157–171.

Brinker, C.J., Hurd, A.J., Schunk, P.R., Frye, G.C., Ashley, C.S., 1992. Review of sol–gel thin film formation. J. Non-Cryst. Solids 147–148, 424–436.

Carretero-Genevrier, A., Drisko, G.L., Grosso, D., Boissiereb, C., Sanchez, C., 2014. Mesoscopically structured nanocrystalline metal oxide thin films. Nanoscale 6, 14025–14043.

Centi, G., Perathoner, S., 2009a. Nano-architecture and reactivity of titania catalytic materials. Part 2. Bidimensional nanostructured films. Catalysis 21, 82–130.

Centi, G., Perathoner, S., 2012. Nanostructured titania thin films for solar use in energy applications. In: Rios, G., Centi, G., Kanellopoulos, N. (Eds), Nanoporous Materials for Energy and the Environment, Pan Stanford, Singapore, pp. 257−282.

Centi, G., Perathoner, S., 2009b. The role of nanostructure in improving the performance of electrodes for energy storage and conversion. Eur. J. Inorg. Chem. 26, 3851–3878.

Chen, H.-S., Huang, S.-H., Perng, T.-P., 2013. Highly transparent hard bio-coating synthesized by low temperature sol–gel process. Surf. Coat. Technol. 233, 140–146.

Chen, R., Wang, J., Wang, H., Yao, W., Zhong, J., 2011. Porous SiO_2/TiO_2 bilayer antireflection coatings with self-cleaning capacity. Adv. Mater. Res. 233–235, 2970–2974.

Chiodo, L., Garc±a-Lastra, J.M., Mowbray, D.J., Iacomino, A., Rubio, A., 2010. Tailoring electronic and optical properties of TiO_2: nanostructuring, doping and molecular-oxide interactions. In: George, T.F., Jelski, D., Letfullin, R.R., Zhang, G. (Eds.), Computational Studies of New Materials II: From Ultrafast Processes and Nanostructures to Optoelectronics, Energy Storage and Nanomedicine. World Scientific Pub., Hackensack, NJ, pp. 301–330., Ch. 12.

Chung, C.J., Hsieh, P.Y., Hsiao, C.H., Lin, H.I., Leyland, A., Matthews, A., He, J.L., 2009. Mutifunctional arc ion plated TiO_2 photocatalytic coatings with improved wear and corrosion protection. Surf. Coat. Technol. 203, 1689–1693.

De Oliveira, R.R.L., Albuquerque, D.A.C., Cruz, T.G.S., Yamaji, F.M., Leite, F.L., 2012. Measurement of the nanoscale roughness by atomic force microscopy: basic principles and applications. In: Bellitto, V. (Ed.), Atomic Force Microscopy – Imaging, Measuring and Manipulating Surfaces at the Atomic Scale. InTech Pub., Rijeka Croatia, pp. 147–174, Ch. 7.

Deubener, J., Helsch, G., Moiseev, A., Bornhöft, H., 2009. Glasses for solar energy conversion systems. J. Eur. Ceram. Soc. 29, 1203–1210.

Dobrzański, L., Drygala, A., 2008a. Development of the laser method of multicrystalline silicon surface texturization. J. Achiev. Mater. Manuf. Eng. 29 (1), 7–14.

Dobrzański, L., Drygala, A., 2008b. Surface texturing of multicrystalline silicon solar cells. J. Achiev. Mater. Manuf. Eng. 31 (1), 77–82.

Dobrzański, L., Drygala, A., Golombek, K., Panek, P., Bielańska, E., Zieba, P., 2008. Laser surface treatment of multicrystalline silicon for enhancing optical properties. J. Mater. Proc. Technol. 201 (1), 291–296.

Dobrzański, L., Szindler, M., 2012. Sol gel TiO_2 antireflection coatings for silicon solar cells. J. Achiev. Mater. Manuf. Eng. 52, 7–14.

Dunuwila, D.D., Gagliardi, D.C., Berglund, A.K., 1994. Application of controlled hydrolysis of titanium(IV) isopropoxide to produce sol–gel-derived thin films. Chem. Mater. 6, 1556–1562.

Faustini, M., Nicole, L., Boissiere, C., Innocenzi, P., Sanchez, C., Grosso, D., 2010. Hydrophobic, antireflective, self-cleaning, and antifogging sol–gel coatings: an example of multifunctional nanostructured materials for photovoltaic cells. Chem. Mater. 22, 4406–4413.

Fleury, B., Dantelle, G., Darbe, S., Boilot, J.P., Gacoin, T., 2012. Transparent coatings made from spray deposited colloidal suspensions. Langmuir 28, 7639–7645.

Fujishima, A., Hashimoto, K., Iyoda, T., Fukayama, S., Yoshimoto, T., Saitoh, T., 2002. Titanium Dioxide Photocatalyst, US Patent 6,387,844 B1.

Fujishima, A., Hashimoto, K., Watanabe, T., 1999. TiO_2 Photocatalysis: Fundamentals and Applications. BKC Inc, Tokyo.

Fujishima, A., Zhang, X., 2006. Titanium dioxide photocatalysis: present situation and future approaches. Comptes Rendus Chimie 9, 750–760.

Gensler, R., Kapitza, H., Zeininger, H., 2013. Self-Cleaning Surface Coating (Photocatalysis), US Patent 8,367,579 B2.

Ghamsari, M.S., Bahramian, A.R., 2008. High transparent sol–gel derived nanostructured TiO_2 thin film. Mater. Lett. 62, 361–364.

Goetzberger, A., Hoffmann, U., 2005. Photovoltaic Solar Energy Generation. Springer, Germany.

Gronet, C., Truman, J., 2007. Self-Cleaning Protective Coatings for Use with Photovoltaic Cells. US Patent 0,017,567.

Guldin, S., Kohn, P., Stefik, M., Song, J., Divitini, G., Ecarla, F., Ducati, C., Wiesner, U., Steiner, U., 2013. Self-cleaning antireflective optical coatings. Nano Lett. 13, 5329–5335.

Harada, T., Murotani, H., Matumoto, S., Honda, H., 2013. Influence of substrate roughness on light scattering of TiO_2 optimal thin films. Chin. Opt. Lett. 11, S10303-1/-4.

Hasan, M.M., Haseeb, A.S.M.A., Masjuki, H.H., Saidur, R., 2010. Adhesion and wear behavior of nanostructured titanium oxide thin film. Int. J. Mech. Mater. Eng. 5, No. 5–10.

Hurd, A.J., 2006. Evaporation and surface tension effects in dip coating. Surf. Sci. Ser. 131, 653–661.

Innocenzi, P., Malfatti, L., 2013. Mesoporous thin films: properties and applications. Chem. Soc. Rev. 42, 4198–4216.

Jaguiro, P., Stsiapanau, A., Hubarevich, A., Mukha, Y., Smirnov, A., 2010. Self-organized nanostructured anodic oxides for display applications. Semicond. Phys., Quant. Electron. Optoelectron. 13, 305–308.

Jin, S.Y., Kim, H.K., Park, J.S., Yoon, H.H., Choi, W.H., 2010. Properties of TiO_2 films prepared for use in dye-sensitized solar cells by using the sol–gel method at different catalyst concentrations. J. Korean Phy. Soc. 57, 1049–1053.

Kaliwoh, N., Zhang, J.-Y., Boyd, I.W., 2002. Characterisation of TiO_2 deposited by photo-induced chemical vapour deposition. Appl. Surf. Sci. 186, 241–248.

Kim, D.J., Hahn, S.H., Oh, S.H., Kim, E., 2002. Influence of calcination temperature on structural and optical properties of TiO_2 thin films prepared by sol–gel dip coating. J. Mater. Lett. 57, 355–360.

Kim, Y.J., Kim, H.J., Lee, M.H., Lim, G.I., Song, H.Y., Choi, Y.S., Park, N.-G., Lee, C., Lee, W.I., 2010. Improvement of photovoltaic efficiency of dye-sensitized solar cell by introducing highly transparent nanoporous TiO_2 buffer layer. J. Nanosci. Nanotech. 10, 340–344.

King, D.M., Du, X., Cavanagh, A.S., Weimer, A.W., 2008. Quantum confinement in amorphous TiO_2 films studied via atomic layer deposition. Nanotechnology 19, 445401, 6pp.

Klobukowski, E.R., Tenhaeff, W.E., McCamy, J.W., Harris, C.S., Narula, C.K., 2013. Atmospheric pressure chemical vapor deposition of high silica SiO_2–TiO_2 antireflective thin films for glass based solar panels. J. Mater. Chem. C: Mater. Opt. Elect. Dev. 1, 6188–6190.

Lai, Y., Tang, Y., Gong, J., Gong, D., Chi, L., Lin, C., Chen, Z., 2012. Transparent superhydrophobic/superhydrophilic TiO_2-based coatings for self-cleaning and anti-fogging. J. Mater. Chem. 22, 7420–7426.

Latthe, S.S., Terashima, C., Nakata, K., Fujishima, A., 2014. Superhydrophobic surfaces developed by mimicking hierarchical surface morphology of lotus leaf. Molecules 19, 4256–4283.
Lee, S.-H., Han, K.-S., Shin, J.-H., Hwang, S.-Y., Lee, H., 2013. Fabrication of highly transparent self-cleaning protection films for photovoltaic systems. Prog. Photovolt: Res. Appl. 21, 1056–1062.
Li, X., He, J., 2013. Synthesis of raspberry-like SiO_2–TiO_2 nanoparticles toward antireflective and self-cleaning coatings. ACS Appl. Mater. Interf. 5, 5282–5290.
Li, X.-M., Reinhoudt, D., Crego-Calama, M., 2007. What do we need for a superhydrophobic surface? A review on the recent progress in the preparation of superhydrophobic surfaces. Chem. Soc. Rev. 36, 1350–1368.
Livage, J., 2004. Basic principles of sol-gel chemistry. In: Aegerter, M.A., Mennig, M. (Eds.), Sol–Gel Technologies for Glass Producers and Users. Springer Pub., pp. 3–14.
Long, M., Wu, D., Cai, W., 2010. Photoinduced hydrophilic effect and its application on self-cleaning technology. Recent Patents Eng. 4, 189–199.
Manea, E., Parvulescu, C.C., Purica, M., Budianu, E., Comanescu, F., 2013. Antireflective coatings with nanostructured TiO_2 thin films for silicon solar cells. J. Nano Res. 21, 89–94.
Mao, P., Chen, J., Zhou, Y., Liao, K., Zhao, B., Han, J., Wang, G., Han, M., 2012. Anisotropy antireflection TiO_2 nanoparticle films fabricated with directed cluster beam deposition. Phys. Status Solidi C: Curr. Topics Solid State Phys. 9, 2366–2369.
Mergel, D., Buschendorf, D., Eggert, S., Grammes, R., Samet, B., 2000. Density and refractive index of TiO_2 films prepared by reactive evaporation. Thin Solid Films 371, 218–224.
Miao, L., Su, L.F., Tanemura, S., Fisher, C.A.J., Zhao, L.L., Liang, Q., Xu, G., 2013. Cost-effective nanoporous SiO_2–TiO_2 coatings on glass substrates with antireflective and self-cleaning properties. Appl. Energy 112, 1198–1205.
Mosaddeq-ur-Rahman, M., Miki, T., Krishna, K.M., Soga, T., Igarashi, K., Tanemura, S., Umeno, M., 1996. Structural and optical characterization of $Pb_xTi_{1-x}O_2$ film prepared by sol-gel method. Mater. Sci. Eng. B 41, 67–71.
Mu, Q., Li, Y., Wang, H., Zhang, Q., 2012. Self-organized TiO_2 nanorod arrays on glass substrate for self-cleaning antireflection coatings. J. Colloid Interf. Sci. 365, 308–313.
Nakamura, M., Kato, S., Aoki, T., Sirghi, L., Hatanaka, Y., 2001. Formation mechanism for TiO_x thin film obtained by remote plasma enhanced chemical vapor deposition in H_2–O_2 mixture gas plasma. Thin Solid Films 401, 138–144.
Nishide, T., Sato, M., Hara, H., 2000. Crystal structure and optical property of TiO_2 gels and films prepared from ti-edta complexes as titania precursors. J. Mater. Sci. 35, 465–469.
Noh, H.N., Myong, S.Y., 2014. Antireflective coating using a WO_3-TiO_2 nanoparticle photocatalytic composition for high efficiency thin-film Si photovoltaic modules. Sol. Energy Mater. Sol. Cells 121, 108–113.
Passalacqua, R., Salvaggio, M.G., Centi, G., Perathoner, S., 2014. Nanostructured two-dimensional titania films for solar fuels and PV applications. Preprints – ACS/Div. Energy Fuels 59, 297–298.
Pelizzetti, E., Sepone, N., 1989. Photocatalysis: Fundamentals and Applications. Wiley, New York.
Perathoner, S., Passalacqua, R., Centi, G., Su, D.S., Weinberg, G., 2007. Photoactive titania nanostructured thin films: synthesis and characteristics of ordered helical nanocoil array. Catal. Today 122, 3–13.
Poulopoulos, P., Baskoutas, S., Pappas, S.D., Garoufalis, C.S., Droulias, S.A., Zamani, A., Kapaklis, V., 2011. Intense quantum confinement effects in Cu_2O thin films. J. Phys. Chem. C 115, 14839–14843.
Prado, R., Beobide, G., Marcaide, A., Goikoetxea, J., Aranzabe, A., 2010. Development of multifunctional sol–gel coatings: antireflection coatings with enhanced self-cleaning capacity. Sol. Energy Mater. Sol. Cells 94, 1081–1088.
San Vicente, G., Morales, A., German, N., Suarez, S., Sanchez, B., 2012. SiO_2/TiO_2 antireflective coatings with photocatalytic properties prepared by sol–gel for solar glass covers. J. Sol. Energy Eng. 134, 041011/1–041011/5.
Schiavello, M., 1988. Photocatalysis and Environment. Trends and Applications. Kluwer Academic Publisher, Dordrecht.
Schneider, J., Matsuoka, M., Takeuchi, M., Zhang, J., Horiuchi, Y., Anpo, M., Bahnemann, D.W., 2014. Understanding TiO_2 photocatalysis: mechanisms and materials. Chem. Rev. 114, 9919–9986.
Seitz, O., Geddes, J.B., Aryal, M., Perez, J., Wassei, J., McMackin, I., Kobrin, B., 2014. Antireflective surface patterned by "rolling mask" lithography. In: Proc. SPIE, 8974 (2014) 89740V/1-89740V/6.
Seo, Y.G., Lee, H., Kim, K., Lee, W., 2010. Transparent thin films of anatase titania nanoparticles with high refractive indices prepared by wet coating process. Mol. Cryst. Liquid Cryst. 520, 477–484.
Shimizu, W., Nakamura, S., Sato, T., Murakami, Y., 2012. Creation of high-refractive-index amorphous titanium oxide thin films from low-fractal-dimension polymeric precursors synthesized by a sol–gel technique with a hydrazine monohydrochloride catalyst. Langmuir 28, 12245–12255.
Singh, M., Pathak, D., Mahajan, A., Bedi, R.K., 2012. Sol gel spin coated TiO_2 films for transparent window applications. J. Optoelectron. Adv. Mater. 14, 624–629.
Smilgies, D.-M., 2009. Scherrer grain-size analysis adapted to grazing incidence scattering with area detectors. J. Appl. Cryst. 42, 1030–1034.
Soler-Illia, G.J.A.A., Angelomé, P.C., Fuertes, M.C., Calvo, A., Wolosiuk, A., Zelcer, A., Bellino, M.G., Martinez, E.D., 2011. Mesoporous hybrid and nanocomposite thin films. A sol–gel toolbox to create nanoconfined systems with localized chemical properties. J. Sol–Gel Sci. Technol. 57, 299–312.
Sreemany, M., Sen, S., 2004. A simple spectrophotometric method for determination of the optical constants and band gap energy of multiple layer TiO_2 thin films. Mater. Chem. Phys. 83, 169–177.
Sreemany, M., Sen, S., 2007. Influence of calcination ambient and film thickness on the optical and structural properties of sol–gel TiO_2 thin films. Mater. Res. Bull. 42, 177–189.
Taga, Y., 2009. Titanium oxide based visible light photocatalysts: materials design and applications. Thin Solid Films 517, 3167–3172.
Uchida, H., Patel, M.N., May, R.Al., Gupta, G., Stevenson, K.J., Johnston, K.P., 2010. Highly-ordered mesoporous titania thin films prepared via surfactant assembly on conductive indium-tin-oxide/-glass substrate and its optical properties. Thin Solid Films 518, 3169–3176.
Wang, M., Ioccozia, J., Sun, L., Lin, C., Lin, Z., 2014. Inorganic-modified semiconductor TiO_2 nanotube arrays for photocatalysis. Energy Environ. Sci. 7, 2182–2202.
Watanabe, A., Tsuchiya, T., Imai, Y., 2002. Selective deposition of anatase and rutile films by KrF laser chemical vapor deposition from titanium isopropoxide. Thin Solid Films 406, 132–137.
Yamamoto, S., Sumita, T., Sugiharuto, T., Miyashita, A., Naramoto, H., 2001. Preparation of epitaxial TiO_2 films by pulsed laser deposition technique. Thin Solid Films 401, 88–93.
Yao, L., He, J., 2014. Facile dip-coating approach to fabrication of mechanically robust hybrid thin films with high transmittance and durable superhydrophilicity. J. Mater. Chem. A: Mater. Energy Sustain. 2, 6994–7003.
Yates Jr, J.T., 2009. Photochemistry on TiO_2: mechanisms behind the surface chemistry. Surf. Sci. 603, 1605–1612.
Ye, L., Zhang, Y., Zhang, X., Hu, T., Ji, R., Ding, B., Jiang, B., 2013. Sol–gel preparation of SiO_2/TiO_2/SiO_2–TiO_2 broadband antireflective coating for solar cell cover glass. Sol. Energy Mater. Sol. Cells 111, 160–164.
Yen, H.-J., Tsai, C.-L., Wang, P.-H., Lin, J.-J., Liou, G.-S., 2013. Flexible, optically transparent, high refractive, and thermally stable polyimide-TiO_2 hybrids for anti-reflection coating. RSC Adv. 3, 17048–17056.
Yu, J., Yu, C.J., Ho, W., Jiang, Z., 2002. Effects of calcination temperature on the photocatalytic activity and photo-induced super-

hydrophilicity of mesoporous TiO_2 thin films. New J. Chem. 26, 607–613.

Zeman, P., Takabayashi, S., 2002. The effect of O_2 partial pressure on the structure and photocatalytic property of TiO_2 films prepared by sputtering. Surf. Coat. Technol. 153, 93–99.

Zhang, D., Yu, W., Hao, D., Li, L., Liu, H., Lu, Z., 2012a. Functional nanostructured surfaces in hybrid sol-gel glass in large area for antireflective and super-hydrophobic purposes. J. Mater. Chem. 22, 17328–17331.

Zhang, H., Fan, D., Yu, T., Wang, C., 2013. Characterization of anti-reflective and self-cleaning SiO_2–TiO_2 composite film. J. Sol–Gel Sci. Technol. 66, 274–279.

Zhang, W., Yang, B., Chen, J., 2012b. Effects of calcination temperature on preparation of boron-doped TiO_2 by sol–gel method. Int. J. Photoenergy 2012, 8 p 528637.

Zhao, X., Zhao, Q., Yu, J., Liu, B., 2008. Development of multifunctional photoactive self-cleaning glasses. J. Non-Cryst. Solids 354, 1424–1430.